Desalination and Water Treatment
www.deswater.com

doi:10.5004/dwt.2017.21368

88 (2017) 154–161
September

Longan seed and mangosteen skin based activated carbons for the removal of Pb(II) ions and Rhodamine-B dye from aqueous solutions

Xiaoting Hong[a,*], Chengran Fang[a], Mengxian Tan[b], Haifeng Zhuang[a], Wanpeng Liu[a], K.S. Hui[c], Zhuoliang Ye[d,*], Shengdao Shan[a], Xianghong Lü[b]

[a]*School of Civil Engineering and Architecture, Zhejiang University of Science and Technology, Key Laboratory of Recycling and Eco-treatment of Waste Biomass of Zhejiang Province, Hangzhou 310023, China, Tel. +86 571 85070528, Fax +86 571 85070143, email: hanren.xiaoting@gmail.com, hongxt@zust.edu.cn (X. Hong), fangchengr@163.com (C. Fang), 286339399@qq.com (H. Zhuang), wpliu@zust.edu.cn (W. Liu), shanshd@vip.sina.com (S. Shan)*
[b]*School of Chemistry & Environment, South China Normal University, Guangzhou 510006, China, email: tanxumong@foxmail.com (M. Tan), xhlu@scnu.edu.cn (X. Lü)*
[c]*School of Mathematics, University of East Anglia, Norwich, NR4 7TJ, UK, email: k.hui@uea.ac.uk (K.S. Hui)*
[d]*School of Chemical Engineering, Fuzhou University, Fuzhou, Fujian 350116, China, email: yezl@fzu.edu.cn (Z. Ye)*

Received 1 February 2017; Accepted 25 August 2017

ABSTRACT

Agricultural biomass wastes of longan seed and mangosteen skin were collected as precursors to prepare activated carbons (LS-AC-5 and MS-AC-5, respectively) through carbonization at medium temperature and KOH activation at high temperature. Their pore structures, structural properties and surface morphologies were characterized by X-ray diffractometer, Brunauer–Emmett–Teller surface measurement system, and scanning electron microscopy, respectively. Effects of contact time and pH on adsorption performances of samples were investigated by removal of Pb(II) ions and Rhodamine-b from aqueous solutions. Experimental adsorption isotherms of Rhodamine-b and Pb(II) ions on LS-AC-5 and MS-AC-5 fitted well with the Langmuir model. Results further showed that MS-AC-5 exhibited a larger surface area of 2960.56 m^2/g and larger portions of micropores and mesopores (pore volume of 1.77 cm^3/g) than LS-AC-5 (surface area: 2728.98 m^2/g; pore volume: 1.39 cm^3/g). Maximum monolayer adsorption capabilities of 1265.82 and 117.65 mg/g for Rhodamine-b and Pb(II) ions on MS-AC-5 were higher than those on LS-AC-5 (1000.20 and 107.53 mg/g), respectively.

Keywords: Activated carbon; Adsorption; Agricultural waste; Pb(II) ions; Rhodamine-b dye

1. Introduction

Rapid growth of developing countries has accelerated the process of water pollution. Each year, mills discharged millions of tons of wastewater containing chemicals such as heavy metals and dyes by. Various treatment techniques, such as adsorption [1–3], membrane filtration [4,5], ion exchange [6], reverse osmosis [7,8], advanced oxidation [9,10], electrochemical methods, precipitation, and coagulation techniques [11], have been used to control the effluents released by mills. Adsorption has long been considered as a highly efficient approach for pollution control through surface forces, complexation, and ion exchange mechanisms [12]. Various adsorbents such as porous carbon [13–16], zeolite [17], resin [18], metal-organic frameworks [19], clay mineral [20] and porous silica [21] have been developed for removal of contaminants from wastewater because of their high availability and efficiency.

Among all the adsorbents, nanostructured porous carbons are of considerable interest owing to their large surface areas, well-developed pore structures, high adsorption capacities, and cost feasibilities. Porous carbons obtained from agricultural biowastes have attracted significant attention because agricultural wastes are recyclable, inexpensive and abundantly available compared with non-renewable

*Corresponding author.

coal-based activated carbons. Agricultural biowastes, which mainly comprise cellulose, lignin and hemicellulose, are also good sources for the production of porous carbon adsorbents, simultaneously offering a solution for comprehensive and high-value utilization of agricultural wastes. Numerous biomasses including coconut shells, seaweeds, corn cobs, rice husks, palm shells, bamboo debris, sugarcane bagasse, fish scales, animal bones, chicken feathers, have been utilized to prepare porous carbons [22–26].

Lead pollution originates mainly from mining, smelting, lead-acid batteries manufacturing, metal plating and finishing, and printing industries. Lead has been proved to be one of the most toxic heavy metals and classified as a human carcinogen with permissible level of 0.015 mg/L in drinking water [27]. Therefore, high demands necessitate the development of effective activated carbon absorbents to eliminate lead ions from wastewaters. Papaya peels were utilized to prepare a novel activated carbon showing a high adsorption capacity for 200 mg/L Pb(II) with a removal rate of 93% in 2 h [28]. Adsorption performance for Pb(II) ions can be successively enhanced by HNO_3 oxidized porous carbons [29]. Maximum adsorption capacity of lead on activated carbon depends on the different sources in the range of 50~112 mg/g [30]. Biomass-derived porous carbon exhibited a selectivity for the removing Pb(II) compared with Cu(II) and Cd(II) from single and binary aqueous solutions via the batch technique [31].

Rhodamine-b pollution can be caused by the printing, textile dyeing, paint, and photographic industries [32] due to its carcinogenicity, neurotoxicity, chronic toxicity, and reproductive toxicity [33]. Although removal of dyes in wastewater by biochemical treatment poses difficulty because of their complex composition and inert properties, adsorption by activated carbon is a particularly effective approach. Lythrum salicaria L-based showed 384.62 mg/g maximum adsorption capacity for rhodamine-b [34]. Porous carbons from by-products of woody biomass gasification and rice husks exhibited low maximum and high maximum adsorption capacities of 189.83 [35] and 518.1 mg/g [36], respectively.

The present study aims to produce activated carbons from agricultural biowastes of longan seed and mangosteen skin through KOH activation. Adsorption performances of these two biomass-derived activated carbons for removal of lead ions and Rhodamine-b from aqueous solution were evaluated based on the physicochemical characteristics of the porous carbons and the operating conditions. Adsorption equilibrium was also explored and fitted by Langmuir and Freundlich adsorption models. Finally, adsorption kinetics was studied by pseudo-first-order and pseudo-second kinetic models to enhance understanding of the adsorption mechanism.

2. Materials and methods

2.1. Materials

This study utilized commercially available chemical reagents. KOH (AR, purity ≥ 85.0%) and HNO_3 (AR, 65%) were purchased from Tianjin Kemiou Chemical Reagent Co., Ltd. Longan seeds and mangosteen skins were collected from a fruit trading center at Guangzhou.

2.2. Synthesis of activated carbons

Longan seeds and mangosteen skins were firstly washed by deioinized water, then oven-dried at 105°C in an oven for 24 h, and finally grounded to biomass powders by an electric pulverizer. Resultant biomass powders were then transferred into corundum boats, which were preliminarily heated in an atmospheric tubular furnace to the target temperature at a heating rate of 3°C/min under Ar atmosphere (flow rate of 20 mL/min) and held at 450°C for 120 min. As-prepared biochar was gridded and then homogeneously mixed with solid KOH at weight ratios of 1:1, 1:4 and 1:5. Thereafter, the mixtures were loaded into a nickel combustion boat and activated in the Ar atmospheric furnace at 800°C for 2 h with a heating rate of 3°C/min and Ar flow rate of 20 mL/min. Then, the activated samples were alternatively washed several times with by 15% HNO_3 and deionized water to remove any inorganic salts or a residual KOH and dried at 110°C for 12 h. Finally, the as-prepared activated carbons were denoted as LS-AC-x and MS-AC-x, respectively, where LS and MS refer to longan seed and mangosteen skin, respectively; AC denotes activated carbon, and x is the weight ratio of biochar to solid KOH.

2.3. Characterization methods

The X-ray diffraction (XRD) patterns were collected using a Bruker D8 advance diffractometer with monochromatic Cu Kα radiation (40 kV, 20 mA) and 2θ angular regions between 10° and 80° were recorded at a scan rate of 0.5°/min. The specific surface areas of the resultant activated carbons were obtained from N_2 adsorption-desorption isotherms on the Micromeritics ASAP 2020 Brunauer–Emmett–Teller (BET) apparatus at liquid nitrogen temperature (77 K). A hybrid nonlocal density functional theory (NLDFT) method was used to investigate the pore size distributions based on the N_2 adsorption isotherms by assuming slit pore geometry for the micropores and cylindrical pore geometry for the mesopores. The nanostructures of the longan seed and mangosteen skin-derived activated carbons were investigated by field emission scanning electron microscopy (FE-SEM, ZEISS Ultra 55).

2.4. Adsorption experiments

Influence of time on the adsorption performance was investigated by separately adding 20 mg adsorbents (LS-AC-5 or MS-AC-5) into 100 mL Rhodamine-b solution (200 mg/L) or Pb(II) solution (10 mg/L) under vigorous stirring at 25°C. Samples were obtained at different time intervals in 120 min. Concentrations of Pb(II) and Rhodamine-B were analyzed by a UV/vis spectrophotometer (UV-1800, Shimadzu Corporation) at 554 nm wavelength and by an atomic absorption spectrophotometer (TAS-986, Beijing Persee Corporation) after filtration through 0.45 μm syringe filters, separately. Effect of the initial pH of the solution on the adsorption was evaluated in the range of 3.0–9.0 through adjusting by 0.1 M KOH or 0.1 M HNO_3. Batch isotherm adsorption experiments were performed by a series of adsorption experiments using 100 mL Rhodamine-b solutions (20~2000) mg/L and 100 mL Pb(II) solutions (5~100 mg/L) in the presence of 20 mg of LS-AC-5 and

MS-AC-5 under vigorous stirring, respectively. Sample concentrations were finally analyzed after 18 h. Langmuir and Freundlich models were used to simulate the adsorption processes. The Langmuir isotherm is applicable to monolayer adsorptions and the Freundlich isotherm expresses adsorption at multilayer and on energetically heterogeneous surface. Langmuir and Freundlich isotherms can be expressed as following Eqs. (1) and (2), respectively:

$$\frac{C_e}{Q_m} = \frac{C_e}{Q_e} + \frac{1}{Q_e K_L} \tag{1}$$

$$\ln Q_m = \ln K_F + \frac{1}{n} \ln C_e \tag{2}$$

where Q_e (mg/g) represents the equilibrium adsorption capacity, C_e (mg/L) refers to equilibrium concentration, Q_m (mg/g) is the maximum adsorption capacity; K_L and K_F correspond to equilibrium adsorption constant for Langmuir and Freundlich models, respectively, and $1/n$ is a measure of adsorption intensity.

3. Results and discussion

Fig. 1 displays FE-SEM images of microstructures of LS-AC-1, LS-AC-4, LS-AC-5, MS-AC-1, MS-AC-4 and MS-AC-5 carbons. Fig. 1a and 1d show that at low KOH-to-biochar ratio, both LS-AC and MS-AC were dominated by macropores for both LS-AC and MS-AC activated carbons. For LS-AC, a number of meso/micropores were generated in the nested cavities on the surfaces with increasing of the KOH-to-biochar ratio, as shown in SEM images from Fig. 1a to Fig. 1c. However, MS-AC exhibited a different morphology that is featured by increasing irregularly shaped nanosheets as the KOH-to-biochar ratio increases as shown in Fig. 1d to 1f. These results indicate that a significant improvement in meso/microporous morphology has occurred in the KOH activation process leading to formation of substantial number of pores composed of randomly oriented microspores or nanosheets. KOH-to-biochar ratio markedly affected porosity and pore structure, with porosity increasing rapidly with increasing ratio owing to severe reactions between carbon surfaces and KOH as activation agent.

Fig. 2 shows the XRD patterns of the as-synthesized LS-AC-1, LS-AC-4, LS-AC-5, MS-AC-1, MS-AC-4 and MS-AC-5, respectively. With the KOH-to-biochar ratio, the diffraction peaks located at 2θ = 26° and 43° which correspond to (002) and (100) planes, respectively, exhibited patterns with a reduced intensity and broadened property. This result indicates that stronger activator leads to a higher percentage of amorphous structure because of the break-

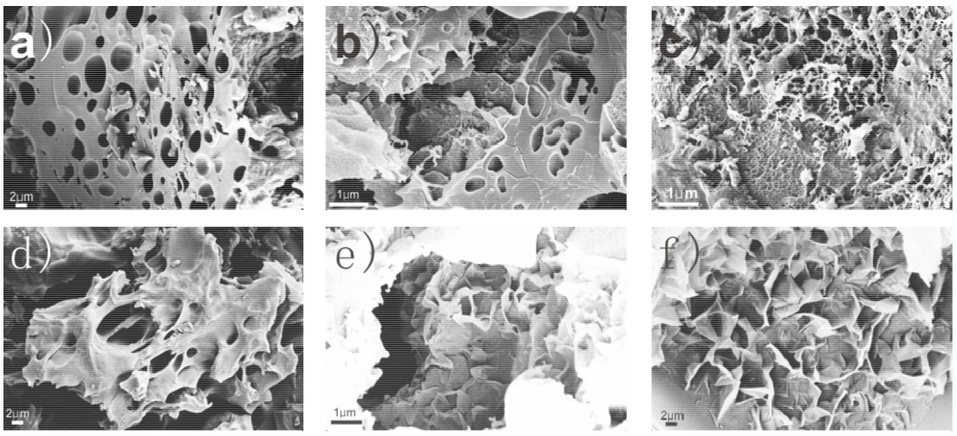

Fig. 1. SEM images of LS-AC-1, LS-AC-4, LS-AC-5, MS-AC-1, MS-AC-4 and MS-AC-5, respectively.

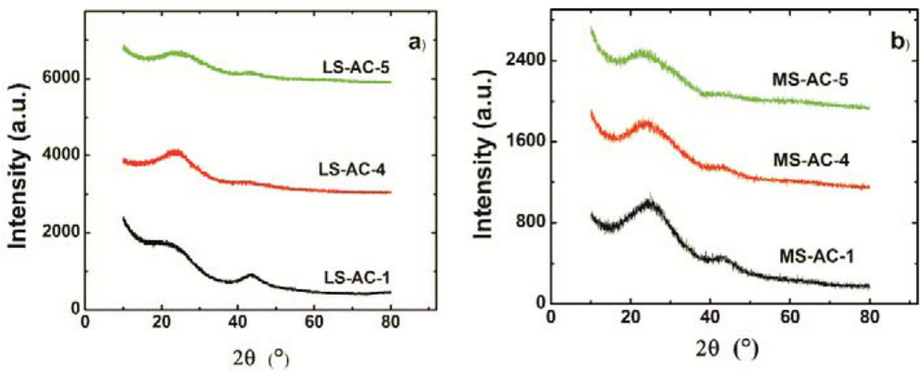

Fig. 2. XRD patterns of LS-AC-1, LS-AC-4, LS-AC-5, MS-AC-1, MS-AC-4 and MS-AC-5, respectively.

down of graphitic crystalline structures during chemical activation.

As shown in Fig. 3, nitrogen adsorption-desorption isotherms were used to investigate the BET surface areas and the porosities of LS-AC and MS-AC. LS-AC-1, LS-AC-4, LS-AC-5, MS-AC-1, MS-AC-4 and MS-AC-5 exhibited type-I N_2 adsorption isotherms showing a steep nitrogen gas uptake at lower relative pressure ($P/P_0 < 0.01$) and a plateau in the intermediate pressure range. These results indicate a microporous nature with a small degree of mesoporosity. Hybrid NLDFT model was used to determine the pore size distribution and total pore volumes by assuming cylindrical-pore geometry for the mesopores and slit-pore geometry for the micropores according to the N_2 isotherm adsorption data. Table 1 summarizes the specific surface areas and pore structures of samples activated with varying KOH-to-biochar. On one hand, for LS-AC, as the ratio of KOH to biochar was increased, the total pore volume increased from 0.47 cm^3/g to 1.39 cm^3/g, BET surface area increased from 803.51 m^2/g to 2728.98 m^2/g, and average pore size decreased from 2.36 nm to 2.04 nm. On the other hand, for MS-AC, as the ratio of KOH to biochar was increased, the total pore volume increased from 0.51 cm^3/g to 1.77 cm^3/g, BET surface area increased from 940.24 m^2/g to 2960.56 m^2/g, and average pore size decreased from 2.19 nm to 1.93 nm. These changes are attributed to the higher percentages of the activation agents that can react with the biochar surface and thus facilitate the formation of abundant micropores. All the samples exhibited a random pore size distribution with several representative peaks centering in the range of < 5 nm. With an increased percentage of the activation agents, biomass-derived porous carbons formed a structure that is predominantly microporous and with peaks centers at 1.1 nm, 0.5 nm and 1.2 nm for LS-AC-5 and MS-AC-5, respectively. This structure resulted from insufficient amount of activation agent for complete carbon activation when KOH-to-carbon ratio is low. With the increasing of the ratio, the activation degree was enhanced, and more pores were formed according to the following reaction of $KOH + C \rightarrow K_2O + CO_2 + 2H_2 + CO + H_2O$. This outcome indicates that activation ratio significantly influences pore size distribution and pore volume.

Figs. 4a and 5a present removal rates (%) of Rhodamine b and Pb(II) ions on LS-AC-5 and MS-AC-5 as a function of contact time. Removal rate of Rhodamine-b was gradually increased with the adsorption time from 22.86% to 76.78% on LS-AC-5 and from 28.59% to 83.16%

Table 1
Specific surface area and pore structure of samples activated with different ratios of potassium hydroxide to biochar

Samples	Surface area ($m^2 \cdot g^{-1}$)	Pore volume ($cm^3 \cdot g^{-1}$)	Average pore size (nm)
LS-AC-1	803.51	0.47	2.36
LS-AC-4	2038.74	1.15	2.09
LS-AC-5	2728.98	1.39	2.04
MS-AC-1	940.24	0.51	2.19
MS-AC-4	2188.30	1.19	2.01
MS-AC-5	2960.56	1.77	1.93

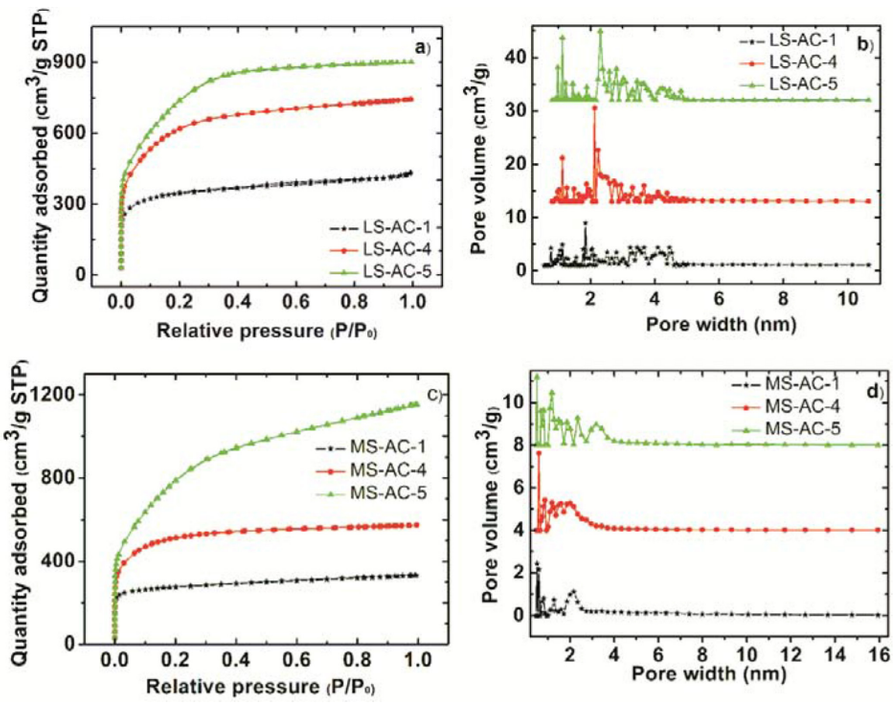

Fig. 3. Nitrogen adsorption-desorption isotherms (a, c) and pore size distribution (b, d) of longan seed and mangosteen skin derived porous carbons, respectively.

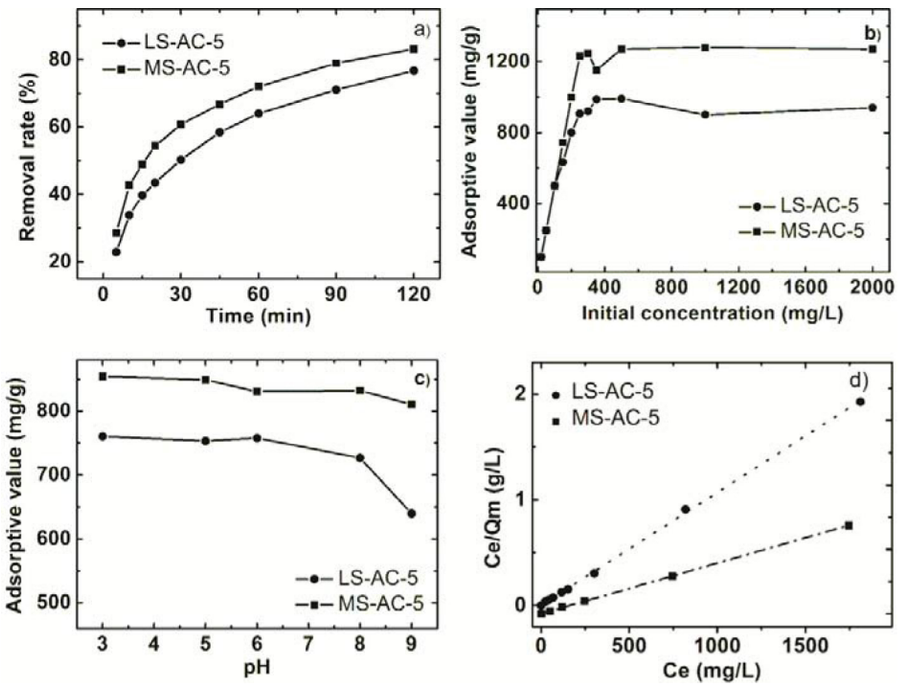

Fig. 4. (a) Effect of contact time of LS-AC-5 and MS-AC-5 for Rhodamine-b adsorption; (b) Adsorption isotherms of Rhodamine-b on LS-AC-5 and MS-AC-5, respectively; (c) Effect of pH on the removal of Rhodamine-b by LS-AC-5 and MS-AC-5; (d) Langmuir fitted curves.

on MS-AC-5 in 120 min, respectively. Pb(II) ions was considerably removed from the aqueous solution at the beginning (<5 min) owing to the high surface areas and high amounts of unoccupied active sites (carboxyl and phenolic hydroxyl groups) on the activated carbons [37,38]. Pb(II) ions adsorption from aqueous solutions by activated carbon was highly affected by solution pH. Figs. 4c and 5c show that the adsorption capacity was increased with increasing pH in the range of 3.0~7.0. As pH increases, the activated carbon surface becomes more negatively charged within the pH range which favorably leading to higher adsorption capacity of cationic charged Pb(II) ions via electrostatic interaction. Analogously, adsorption value was relatively low at pH of 3, possibly because of electrostatic repulsion between cationic charged Pb(II) ions and the hydrogen ions that were released from phenolic hydroxyl groups in the adsorption process. However, the pH of the solution slightly influenced Rhodamine-b adsorption process with the exception at high pH of 9, this result is be inconsistent with adsorption behaviors on other adsorbents with extremely low surface area [39]. This finding infers that high surface area completely dominates during the adsorption compared with surface charge of the adsorbents. Figs. 4b and 5b compare adsorption isotherms of Rhodamine-b and Pb(II) ions on LS-AC-5 and MS-AC-5. As depicted from the plots in Figs. 4d and 5d, the values of the Langmuir isotherm model fit well the experimental data with square of correlations higher than 0.999 indicating a monolayer coverage of adsorbent surface [40]. Table 2 provides isotherm parameters for the Langmuir isotherm model. Maximum adsorption capacities (Q_m, mg/g) of LS-AC-5 for Rhodamine-b and Pb(II) ions reaches 1000.20 mg/g and 107.53 mg/g, and for MS-AC-5, 1265.82 mg/g and 117.65 mg/g, respectively. With its higher surface area and pore volume, MS-AC-5 yielded higher removal efficiencies of Rhodamine b and Pb(II) ions than those on LS-AC-5.

Studies of adsorption kinetics can enhance the understanding of the adsorption mechanism. Adsorption kinetics is a physical–chemical process that involves the mass transfer and adsorption rate of a solute (adsorbate) from the fluid phase to the active sites of the adsorbents. To study the adsorption kinetics and mechanism of Rhodamine-b and Pb(II) ions on biomass-derived activated carbons, pseudo-first-order equation and pseudo-second-order equation were used to fit the experimental results.

The pseudo-first-order equation is as follows:

$$q_t = q_e(1 - e^{-k_1 t}) \tag{3}$$

The pseudo-second-order equation is expressed using the following:

$$q_t = \frac{k_2 q_e^2 t}{1 + k_2 q_e t} \tag{4}$$

where q_t (mg·g^{-1}) represent adsorption capacity for Pb(II) ions and Rhodamine-b adsorption capability at a specific time of t (min) and q_e (mg·g^{-1}) is the equilibrium adsorption capacity; k_1 (min^{-1}) and k_2 (g·mg^{-1}·min^{-1}) depict rate constants of pseudo-first-order equation and pseudo-second-order equation, respectively.

Fig. 6a and 6b show the experimental adsorption kinetics curves and fitting curves of both Pb(II) ions and

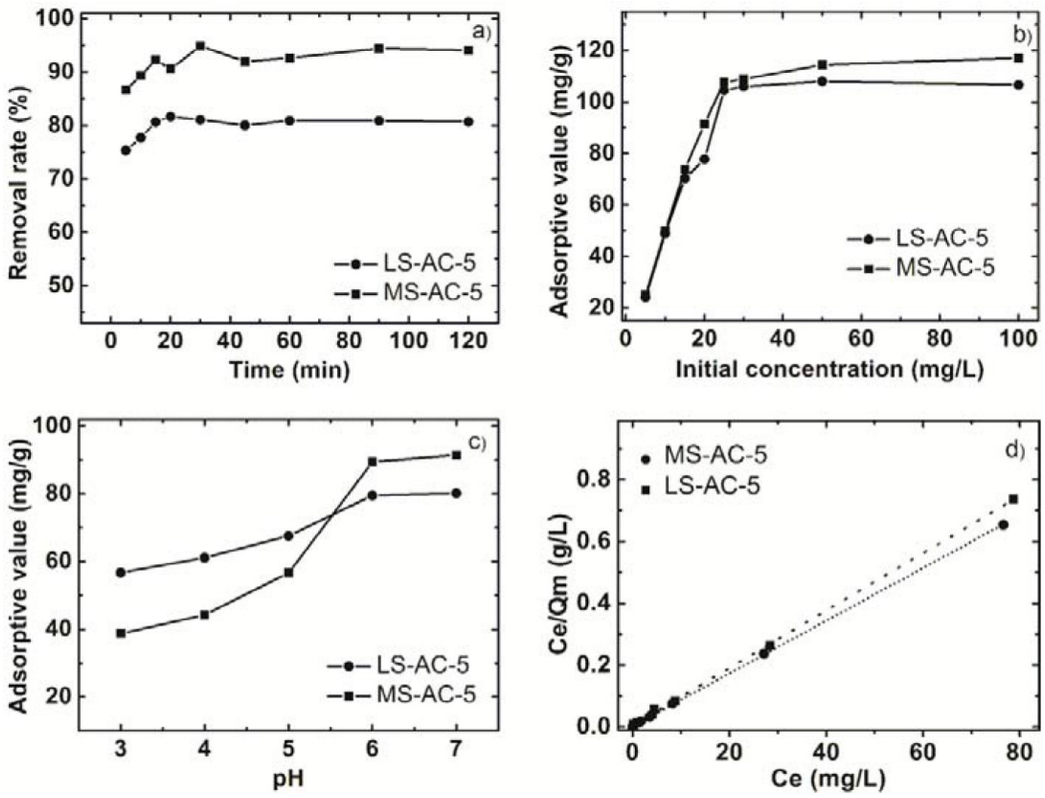

Fig. 5. (a) Effect of contact time of LS-AC-5 and MS-AC-5 for Pb(II) ions adsorption; (b) Adsorption isotherms of Pb(II) ions on LS-AC-5 and MS-AC-5, respectively; (c) Effect of pH on the removal of Pb(II) ions by LS-AC-5 and MS-AC-5 ; (d) Langmuir fitted curves.

Table 2
Isotherm adsorption parameters Rhodamine-b and Pb(II) ions on MS-AC-5 and LS-AC-5, respectively

Model	Langmuir model			Freundlich model		
	Q_m (mg/g)	K_L (L/mg)	R^2	n	K_F (mg$^{1-1/n}$/g·L$^{1/n}$)	R^2
Pb(II) ions on LS-AC-5	107.53	2.04	0.9995	4.86	57.35	0.6735
Pb(II) ions on MS-AC-5	117.65	3.33	0.9999	7.19	78.26	0.8877
RB on LS-AC-5	1000.20	0.47	0.9994	12.44	322.14	0.4253
RB on MS-AC-5	1265.82	0.69	0.9999	6.26	522.91	0.4144

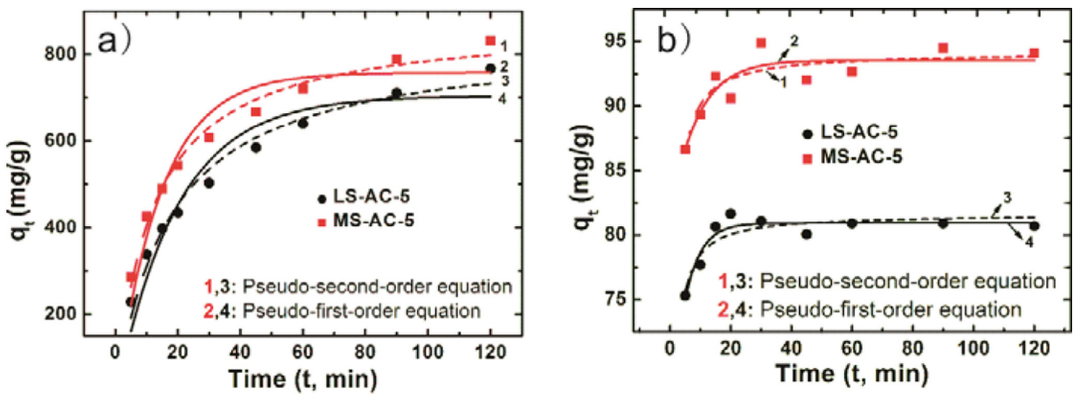

Fig. 6. Adsorption kinetics data and fitted models of (a) Rhodamine-b and (b) Pb(II) ions onto LS-AC-5 and MS-AC-5, respectively.

Table 3
Kinetic parameters for Rhodamine-b and Pb(II) ions adsorption on MS-AC-5 and LS-AC-5, respectively

Kinetic model	Pseudo-first -order			Pseudo-second -order		
	k_1 (min^{-1})	q_e (mg/g)	R^2	k_1 (g/mg·min)	q_e (mg/g)	R^2
Pb(II) ions on LS-AC-5	0.5343	80.58	0.721	0.0309	81.65	0.813
Pb(II) ions on MS-AC-5	0.5338	92.67	0.529	0.0235	94.19	0.807
RB on LS-AC-5	0.0514	704.37	0.915	7.0968×10^{-5}	835.87	0.978
RB on MS-AC-5	0.0690	758.71	0.907	9.7796×10^{-5}	876.62	0.985

Rhodamine-b onto LS-AC-5 and MS-AC-5 at 25°C, respectively. The adsorption of Pb(II) ions and Rhodamine-b by the activated carbons rapidly occurred in the range of 20~40 min because of the rapid occupation of easily accessible external surface adsorption sites through outer sphere complexation. Subsequently, the adsorption capacity stabilized due to the formation of inner layer complexes. As shown in Table 3, the correlation coefficients (R^2) of the pseudo-second-order equation exceeds that of the pseudo-first-order equation indicating that the kinetic adsorption process could be described better by the pseudo-second-order kinetic model. Given that it explains the external liquid film diffusion, surface adsorption and intra-particle diffusion processes [41], the pseudo-second-order model confirmed that chemisorption is the rate-limiting step in kinetic adsorption [42].

4. Conclusions

Two types of activated carbons were prepared from fruit-biomass wastes by chemical activation with KOH. These activated carbons were characterized in terms of surface and structural properties, and then used to remediate the contamination of Rhodamine-b and Pb(II) in aqueous solutions. MS-AC possessed larger specific surface area, pore volume and smaller average pore size in comparison with LS-AC. Experimental adsorption equilibrium curves of Rhodamine-b and Pb(II) on LS-AC-5 and MS-AC-5 were well fitted by the Langmuir isotherm model. MS-AC-5 presented the highest adsorption capability for the removal of Rhodamine-b and Pb(II) ions from aqueous solutions, with maximum adsorption capacities of 1265.82 and 117.65 mg/g, respectively; these results were mainly attributed to its higher surface area and higher number of micropores. Effects of solution pH on the adsorption amount of Pb(II) ions was markedly stronger than that of Rhodamine-b.

Acknowledgements

Financial support for this work was provided by the National Key R&D Program of China (13th Five Year Plan, 2017YFD061006), Natural Science Foundation of Zhejiang Province (Y18E080055), Major Science and Technology Projects of Zhejiang Province (2015C02037), and Fuzhou University Qishan Scholar [Oversea project, grant number XRC-1508].

References

[1] A. Wołowicz, Z. Hubicki, Carbon-based adsorber resin Lewatit AF 5 applicability in metal ion recovery, Micropor. Mesopor. Mater., 224 (2016) 400–414.
[2] A. Habineza, J. Zhai, T. Ntakirutimana, F.P. Qiu, X. Li, Q. Wang, Heavy metal removal from wastewaters by agricultural waste low-cost adsorbents: hindrances of adsorption technology to the large scale industrial application – a review, Desal. Water Treat., 78 (2017) 192–214.
[3] S. Guergazi, S. Hamzaoui, S. Achour, Effect of the mineralization on removing the humic substances by adsorption on activated carbon, Desal. Water Treat., 78 (2017) 127–131.
[4] M. Cakmakci, A.B. Baspinar, U. Balaban, V. Uyak, I. Koyuncu, C. Kinaci, Comparison of nanofi ltration and adsorption techniques to remove arsenic from drinking water, Desal. Water Treat., 9 (2009) 149–154.
[5] F.H. Chi, W.P. Cheng, D.R. Tian, R.F. Yu, C.H. Fu, Potassium alum crystal derived from aluminum salt in water treatment sludge by nanofiltration, J. Mater. Cycles Waste Manage., 17 (2015) 522–528.
[6] M.B. Abda, O. Schäf, Y. Zerega, Ion exchange effect on asymmetric dioxins adsorption onto FAU-type X-zeolites, Micropor. Mesopor. Mater., 217 (2015) 178–183.
[7] Z. Xu, J. Liu, Z. Huang, X. Yang, S. Wang, F. Fang, S. Chen, Y. Wang, Experimental study of a stand-alone solar-wind powered reverse osmosis seawater desalination system, Desal. Water Treat., 78 (2017) 24–33.
[8] V. Colla, T.A. Branca, F. Rosito, C. Lucca, B.P. Vivas, V.M. Delmiro, Sustainable reverse osmosis application for wastewater treatment in the steel industry, J. Cleaner Prod., 130 (2016) 103–115.
[9] C. Zhang, M. Jin, J. Tang, X. Gao, Removal of cyclic volatile methylsiloxanes in effluents from treated landfill leachate by electrochemical oxidation, J. Mater. Cycles Waste Manage., 2016 (2016) 1–5.
[10] M. Ginni, S.A. Kumar, J.R. Banu, I.T. Yeom, Synergistic photodegradation of pulp and paper mill wastewater by combined advanced oxidation process, Desal. Water Treat., 68 (2017) 160–169.
[11] L.F. Silva, A.D. Barbosa, H.M. Paula, L.L. Romualdo, L.S. Andrade, Treatment of paint manufacturing wastewater by coagulation/electrochemical methods: Proposals for disposal and/or reuse of treated water, Water Res., 101 (2016) 467–475.
[12] X. Peng, F. Hu, F.L.Y. Lam, Y. Wang, Z. Liu, H. Dai, Adsorption behavior and mechanisms of ciprofloxacin from aqueous solution by ordered mesoporous carbon and bamboo-based carbon, J. Colloid Interface Sci., 460 (2015) 349–360.
[13] W.H. Chan, M.N. Mazlee, Z.A. Ahmad, M.A.M. Ishak, J.B. Shamsul, The development of low cost adsorbents from clay and waste materials: a review, J. Mater. Cycles Waste Manage., 2015 (2015) 1–14.
[14] K. Li, Z. Wan, J. Li, M. Lu, X. Wang, Amino-functionalized bimodal ordered mesoporous carbon with high surface area for efficient adsorption of lead (II) ions, Desal. Water Treat., 60 (2017) 200–211.

[15] L.W. Yam, L. Lim, S. Hosseini, T.S.Y. Choong, Enhancement of phenol adsorption on mesoporous carbon monolith modified by NaOH and NH_3: equilibrium and kinetic studies, Desal. Water Treat., 57 (2016) 4183–4193.
[16] N. Tahri, I. Jedidi, S. Ayadi, S. Cerneaux, M. Cretin, R.B. Amar, Preparation of an asymmetric microporous carbon membrane for ultrafiltration separation: application to the treatment of industrial dyeing effluent, Desal. Water Treat., 57 (2016) 23473–23488.
[17] L. Wang, C. Han, M.N. Nadagouda, D.D. Dionysiou, An innovative zinc oxide-coated zeolite adsorbent for removal of humic acid, J. Hazard. Mater., 313 (2016) 283–290.
[18] K. Li, H. Liang, F. Qu, S. Shao, H. Yu, Z. Han, X. Du, G. Li, Control of natural organic matter fouling of ultrafiltration membrane by adsorption pretreatment: Comparison of mesoporous adsorbent resin and powdered activated carbon, J. Membr. Sci., 471 (2014) 94–102.
[19] N. Yin, K. Wang, L. Wang, Z. Li, Amino-functionalized MOFs combining ceramic membrane ultrafiltration for Pb (II) removal, Chem. Eng. J., 306 (2016) 619–628.
[20] Y. Lyu, X. Su, S. Zhang, Y. Zhang, Preparation and characterization of La(III)-Al(III) Co-loaded hydrothermal palygorskite adsorbent for fluoride removal from groundwater, Water Air Soil Pollut., 2016 (2016) 227–454.
[21] F. Liu, Z. Wu, D. Wang, J. Yu, X. Jiang, X. Chen, Magnetic porous silica–graphene oxide hybrid composite as a potential adsorbent for aqueous removal of p-nitrophenol, Colloids Surfaces A: Physicochem. Eng. Asp., 490 (2016) 207–214.
[22] X.T. Hong, K.S. Hui, Z. Zeng, K.N. Hui, L. Zhang, M. Mo, M. Li, Hierarchical nitrogen-doped porous carbon with high surface area derived from endothelium corneum gigeriae galli for high-performance supercapacitor, Electrochim. Acta, 130 (2014) 464–469.
[23] A. Bhatnagar, F. Kaczala, W. Hogland, M. Marques, C.A. Paraskeva, V.G. Papadakis, M. Sillanpää, Valorization of solid waste products from olive oil industry as potential adsorbents for water pollution control-a review, Environ. Sci. Pollut. Res., 21 (2014) 268–298.
[24] A. Garba, N.S. Nasri, H. Basri, R. Ismail, Z.A. Majid, U.D. Hamza, J. Mohammed, Adsorptive removal of phenol from aqueous solution on a modified palm shell based carbon: fixed-bed adsorption studies, Desal. Water Treat., 57 (2016) 29488–29499.
[25] I. Demiral, C.A. Samdan, H. Demiral, Production and characterization of activated carbons from pumpkin seed shell by chemical activation with $ZnCl_2$, Desal. Water Treat., 57 (2016) 2446–2454.
[26] N. Mohanraj, S. Bhuvaneshwari, Decolorization of eosin-Y dye using activated carbon electrode prepared from bael fruit (Aegle marmelos) shell, Desal. Water Treat., 65 (2017) 233–242.
[27] H. Liu, P. Dai, J. Zhang, C. Zhang, N. Bao, C. Cheng, L. Ren, Preparation and evaluation of activated carbons from lotus stalk with trimethyl phosphate and tributyl phosphate activation for lead removal, Chem. Eng. J., 228 (2013) 425–434.
[28] S. Abbaszadeh, S.R.W. Alwi, C. Webb, N. Ghasemi, I.I. Muhamad, Treatment of lead-contaminated water using activated carbon adsorbent from locally available papaya peel biowaste, J. Cleaner Prod., 118 (2016) 210–222.
[29] H.C. Tao, H.R. Zhang, J.B. Li, W.Y. Ding, Biomass based activated carbon obtained from sludge and sugarcane bagasse for removing lead ion from wastewater, Bioresour. Technol., 192 (2015) 611–617.
[30] L. Largitte, T. Brudey, T. Tant, P.C. Dumesnil, P. Lodewyckx, Comparison of the adsorption of lead by activated carbons from three lignocellulosic precursors, Micropor. Mesopor. Mater., 219 (2016) 265–275.
[31] T. Bohli, A. Ouederni, N. Fiol, I. Villaescusa, Evaluation of an activated carbon from olive stones used as an adsorbent for heavy metal removal from aqueous phases, Comptes Rendus Chimie., 18 (2015) 88–99.
[32] M. Das, K.G. Bhattacharyya, Oxidation of Rhodamine B in aqueous medium in ambient conditions with raw and acid-activated MnO_2, NiO, ZnO as catalysts, J. Mol. Catal. A: Chem., 391 (2014) 121–129.
[33] R. Nagaraja, N. Kottam, C.R. Girija, B.M. Nagabhushana, Photocatalytic degradation of Rhodamine B dye under UV/solar light using ZnO nanopowder synthesized by solution combustion route, Powder Technol., 216 (2012) 91–97.
[34] Y. Huang, X. Zheng, S. Feng, Z. Guo, S. Liang, Enhancement of rhodamine B removal by modifying activated carbon developed from Lythrum salicaria L. with pyruvic acid, Colloids Surfaces A: Physicochem. Eng. Asp., 489 (2016) 154–162.
[35] T. Maneerung, J. Liew, Y. Dai, S. Kawi, C. Chong, C.H. Wang, Activated carbon derived from carbon residue from biomass gasification and its application for dye adsorption: Kinetics, isotherms and thermodynamic studies, Bioresour. Technol., 200 (2016) 350–359.
[36] L. Ding, B. Zou, W. Gao, Q. Liu, Z. Wang, Y. Guo, X. Wang, Y. Liu, Adsorption of Rhodamine-B from aqueous solution using treated rice husk-based activated carbon, Colloids Surfaces A: Physicochem. Eng. Asp., 446 (2014) 1–7.
[37] S. Yao, J. Zhang, D. Shen, R. Xiao, S. Gu, M. Zhao, J. Liang, Removal of Pb(II) from water by the activated carbon modified by nitric acid under microwave heating, J. Colloid Interface Sci., 463 (2016) 118–127.
[38] M. Barczak, K. Michalak-Zwierz, K. Gdula, K. Tyszczuk-Rotko, R. Dobrowolski, A. Dąbrowski, Ordered mesoporous carbons as effective sorbents for removal of heavy metal ions, Micropor. Mesopor. Mater., 211 (2015) 162–173.
[39] A.A. Inyinbor, F.A. Adekola, G.A. Olatunji, Kinetics, isotherms and thermodynamic modeling of liquid phase adsorption of Rhodamine B dye onto Raphia hookerie fruit epicarp, Water Resourc. Indust., 15 (2016) 14–27.
[40] R. Zhu, Q. Chen, Q. Zhou, Y. Xi, J. Zhu, H. He, Adsorbents based on montmorillonite for contaminant removal from water: A review, Appl. Clay Sci., 123 (2016) 239–258.
[41] V. Vadivelan, K.V. Kumar, Equilibrium, kinetics, mechanism, and process design for the sorption of methylene blue onto rice husk, J. Colloid Interface Sci., 286 (2005) 90–100.
[42] Y. Sun, C. Ding, W. Cheng, X. Wang, Simultaneous adsorption and reduction of U (VI) on reduced graphene oxide-supported nanoscale zerovalent iron, J. Hazard. Mater., 280 (2014) 399–408.